Received: 24 February 2018 | Accepted: 5 March 2018

DOI: 10.1111/ijac.12897

SPECIAL ISSUE ARTICLE

International Journal of Applied Ceramic TECHNOLOGY

Synthesis and characterization of silica-coated superparamagnetic iron oxide nanoparticles and interaction with pancreatic cancer cells

Cristina Multari[1] | **Marta Miola**[1] | **Sara Ferraris**[1] | **Dania Movia**[2] | **Kristina Žužek Rožman**[3] | **Nina Kostevšek**[3] | **Antonia Follenzi**[4] | **Enrica Verné**[1] | **Adriele Prina-Mello**[2,5]

[1]Department of Applied Science and Technology, Politecnico di Torino, Torino, Italy

[2]Department of Clinical Medicine/Trinity Translational Medicine Institute (TTMI), Trinity College Dublin, Dublin, Ireland

[3]Department of Nanostructured Materials, Jožef Stefan Institute, Ljubljana, Slovenia

[4]Department of Health Sciences, Università del Piemonte Orientale "A. Avogadro", Novara, Italy

[5]AMBER Centre, CRANN Institute, Trinity College Dublin, Dublin, Ireland

Correspondence
Adriele Prina-Mello
Email: prinamea@gmail.com

Funding information
MULTIFUN project "Development of nanotechnology-based systems for detection, diagnosis and therapy for cancer", Grant/Award Number: 262943; AIRC Grant 2012 "Development of engineered magnetic nanoparticles for cancer therapy", Grant/Award Number: 13166; S. Paolo Grant "CSP-Torino-Piemonte" 2012 "Development of engineered magnetic nanoparticles for targeted therapies (LV-MNPs)", Grant/Award Number: 12-CSP-C04-018

Abstract

The aim of the study is to investigate the relationship between the physico-chemical properties of superparamagnetic iron oxide nanoparticles (SPIONs) and their cytotoxicity profile in light of their potential biomedical application as nanocarriers for pancreatic cancer treatment. Two types of SPIONs were tested: magnetite nanoparticles (Fe_3O_4 NPs) and silica-coated magnetite nanoparticles (SiO_2-Fe_3O_4 NPs). The physico-chemical properties of the 2 SPIONs were characterized by means of Dynamic Light Scattering (DLS), Transmission Electron Microscopy (TEM), Energy Dispersive X-ray Spectrometry (EDS), and Selected Area Electron Diffraction (SAED). Their magnetic properties were quantified as magnetization saturation (Ms) and Remanence. The colloidal stability was investigated by Isoelectric Point Measurements and sedimentation tests. Finally, in vitro characterizations were performed to quantify the half maximal lethal concentration (LC_{50}), by means of High Content Screening Analysis (HCSA), Flow cytometry (FC), and Laser Scanning Confocal Microscopy (LSCM). The obtained NPs present a spherical shape and a dimension between 10 and 20 nm, a superparamagnetic behavior and surface charge in agreement with their surface chemistry. The in vitro tests demonstrate that both NPs induce similar levels of cytotoxicity in a PANC-1 cell model and were internalized, with SiO_2-Fe_3O_4 NPs associated to a slightly higher cellular internalization, probably due to their higher dispersability.

KEYWORDS
magnetic materials/properties, nanomaterials, nanoparticles

1 | INTRODUCTION

The use of magnetic nanoparticles (NPs) for biomedical applications is a novel and highly interdisciplinary field, offering great potential in therapeutics and diagnostics, both in vitro and in vivo. NPs possessing magnetic properties offer great advantages because they can provide selective attachment to a functional molecule, confer magnetic properties to the target, and allow manipulation and transport to a desired location through the control of an external magnetic field produced by an electromagnet or permanent

Multari and Miola are joint first name author.
Follenzi and Verné are joint senior.

magnet.[1] Magnetic properties depend on size, shape, structure, and crystallinity of the NPs.[2] The synthesis method, affecting the above-mentioned features, indirectly influences the magnetic properties. Moreover, surface chemistry has a role on the in vitro and in vivo performances of NPs. Magnetic NPs also display the phenomenon of supermagnetism, which offers advantage of reducing the risk of particles aggregation.[3] Due to superparamagnetic properties, the susceptibility of these NPs when placed in an external magnetic field is very low and they do not retain any net magnetization once the external magnetic field is removed. This property is typically associated with a Fe_3O_4 NPs core size in the 3-50 nm[4] range.

Super Paramagnetic Iron Oxide Nanoparticles, referred from here onwards as SPIONs, have emerged as one of the most appealing candidates for cancer diagnosis and therapy.[5] SPIONs, present a higher performance in terms of chemical colloidal stability and biocompatibility as compared to other metallic NPs.[6] The advantage of being colloidally stable is that aggregation of a stable dispersion can be neglected.

In literature there are several reports on the potential use of SPIONs for biomedical application[7]; however, the scientific community is still collecting experimental results about their biocompatibility and biodistribution, which are still not completely assessed. It is known[8] that the biological impact of these nano-carriers can differ as a function of the cell type tested, showing to be safe for some cell lines and toxic for others. Thus, the assessment of the biological impact of SPIONs on various cell lines is still an open issue, which should be further investigated to assist the development of any theranostics applications of SPIONs, such as nanoprobe for Magnetic Resonance Imaging (MRI), magnetic heating for cancer hyperthermia treatment, magnetofection. Many works in literature focus on magnetite NPs (Fe_3O_4 NPs) and silica-coated magnetite NPs (SiO_2-Fe_3O_4 NPs). The magnetic core (Fe_3O_4) makes their localization in the human organism controllable, while the silica shell should provide stability and poly-functionality, being silica an optimal substrate for functionalization with a variety of biologically active ligands.[9] Some of the authors of this work have already assessed the biocompatibility of Fe_3O_4 NPs and SiO_2-Fe_3O_4 NPs on endothelial cells,[10] their effect on mouse breast cancer 4T1 cells and on pancreatic islet endothelial MS1 cells.[11] The NPs tumor targeting ability was also assessed by coupling with Lentiviral Vectors.[12,13] Catalano et al[10] performed direct and indirect cytotoxicity assays, ROS generation, and apoptosis enzymes activation tests, demonstrating that both Fe_3O_4 and Fe_3O_4-SiO_2 NPs are cytocompatible, in a concentration-dependent mode, in a mouse endothelial cell line. Muzio et al[11] investigated the biological responses (viability and internalization) triggered by Fe_3O_4 and Fe_3O_4-SiO_2 NPs (unfunctionalized or conjugated with linoleic acid) in mouse breast cancer 4T1 cells and pancreatic islet endothelial MS1 cells (a nontumorigenic sinusoidal endothelial cell line derived from pancreas). Finally, in MS1 cells Borroni et al[13] demonstrated that slight or no reduction in cell viability was induced by exposure to Fe_3O_4 or Fe_3O_4-SiO_2 NPs.

The aim of this study was to evaluate the biological behavior and toxicity of this family of NPs against a pancreatic cell line (PANC-1 cells), as further step of the investigation on the effect of these nano-carriers in pancreatic cells, in view of the potential use of such nanomaterials as tools for the diagnosis and therapy of pancreatic cancer. In literature, various studies describe the response of pancreatic cancer cells when exposed to a range of nanoparticles types.[14-17] To the author's best knowledge, however, studies on the biological response of PANC-1 cell line exposed to Fe_3O_4 NPs and SiO_2-Fe_3O_4 NPs are still lacking. Moreover, most of the available research papers are focused on the efficacy of magnetic nanoparticles in hyper-thermic treatments or drug loaded magnetic nanoparticles.[18] On the contrary, few studies estimate the interaction and toxicity of magnetic NPs toward this cell line. In the past 10 years, pancreatic cancer had a high mortality rate all over the world according to the cancer statistic 2017[19] which accounts for over 40 000 deaths annually only in the United States and about 80 000 in Europe.

2 | MATERIALS AND METHODS

2.1 | Synthesis of Fe_3O_4 and SiO_2-Fe_3O_4 NPs

Iron oxide nanoparticles (Fe_3O_4 NPs) and silica-coated iron oxide nanoparticles (SiO_2-Fe_3O_4 NPs) were synthesized as reported in Refs[11,13] and suspended in H_2O. All reagents were purchased from Sigma-Aldrich, unless otherwise specified in the text.

Briefly, aqueous solution of Fe^{2+} and Fe^{3+} salts in a 1:2 molar ratio was prepared by mixing $FeCl_2*4H_2O$ and $FeCl_3*6H_2O$ in bi-distilled water under magnetic agitation. Fe_3O_4 precipitation occurred by adding NH_4OH drop by drop, until the pH of the mixture reached about 10 and the solution turned to black. In order to break eventual agglomerates, the solution was put in an ultrasound bath for 20 minutes. Finally, the Fe_3O_4 NPs were washed with bi-distilled water to remove the unreacted reagents, observing a decrease in the pH. After the washing step, SPIONs were re-suspended in a 0.05 mol/L solution of citric acid (CA) and the pH adjusted to 5.2 by adding NH_4OH dropwise. The suspension was kept 90 minutes at room temperature in orbital shaker (KS 4000i control, IKA®) at 150 rpm. This step was necessary to allow the

deprotonation of 2 carboxylic groups of CA and their bonding to the -OH groups exposed by Fe_3O_4 NPs.[20] The as obtained CA capped Fe_3O_4 NPs were washed with bi-distilled water in an ultrafiltration device (Solvent Resistant Stirred Cells - Merck Millipore) and re-suspended in bi-distilled water, adjusting the pH at about 10. This step induced the deprotonation of the third carboxylic group of CA, allowing a finest Fe_3O_4 NPs dispersion. Finally, Fe_3O_4 NPs were coated with a silica shell following the Stöber method.[21] CA stabilized Fe_3O_4 NPs were suspended in a mixture of Tetraethyl orthosilicate (TEOS as silica precursor), ethanol and water (with an ethanol: water ratio of 1:1) and stirred for 3 hours at 25°C and 150 rpm. An amount of 0.002 mL of TEOS/mg of magnetic nanoparticles was used. Subsequently, SiO_2-Fe_3O_4 NPs were washed with bi-distilled water using the ultrafiltration device and re-dispersed in water. Finally, the as obtained SiO_2-Fe_3O_4 NPs were washed with bi-distilled water using the ultrafiltration device and re-dispersed in water.

2.2 | Characterization of Fe_3O_4 and SiO_2-Fe_3O_4 NPs

2.2.1 | Morphology, phase analysis, and colloidal stability

Both kinds of NPs have been characterized by Transmission Electron Microscopy (TEM, Jeol JEM-2100, operating at 200 kV) equipped with Energy Dispersive X-ray Spectrometry (EDXS) in imaging selected area electron diffraction (SAED) mode to assess their shape, morphology, size, and composition. Samples for the TEM analysis were prepared by adding a drop of NPs suspension on lacey, carbon-coated TEM grid.

Nanoparticle Tracking Analysis (NTA; Malvern Instruments, UK) was used to determine the concentrations of the nanoparticles suspensions. NTA measurements were carried out diluting Fe_3O_4 NPs and SiO_2-Fe_3O_4 NPs in water, with a dilution factor of 1×10^4, at 25°C. All the measurements were repeated for 5 cycles of 60 seconds each and the final concentrations have been expressed as an average of all detected ones, according to previously reported protocols.[22,23]

The colloidal stability was investigated by sedimentation test and by zeta potential measurements. The sedimentation test was carried out by applying a permanent magnet on the bottom of the suspension flasks. Both naked Fe_3O_4 and CA capped Fe_3O_4 were examined at $t = 0$ and $t = 48$ hours by leaving the suspension on the magnet for the entire duration of the test.

The zeta potential measurements were performed as a function of pH, using a laser-scattering method (ZetaPALS potential analyzer, Brookhaven, USA). The particles were diluted 1:100 with deionized water before measurement which was repeated 3 times per sample at room temperature.

The hydrodynamic radius of NPs was determined by Dynamic Light Scattering (DLS Zetasizer Nano S particle analyzer, Malvern Instruments). Ten measurements of 300 seconds for each sample were processed. The following parameters were set during the measurement according to the properties of the solvents and material to be measured: Refractive Index 2.42, Absorption 0.200, Viscosity 0.99 cp, Water Refractive index 1.330.

2.2.2 | Magnetic properties

The superparamagnetic behavior and the magnetic saturation of the NPs was evaluated with a Vibrating Samples Magnetometer (VSM) MicroSense model FCM 10, operated at room temperature in the field range −15 kOe to 15 kOe. Suspension of NPs was dried to obtain NPs in a powder form and obtained magnetization signal was normalized by the mass of the sample.

2.3 | In vitro test

Human pancreatic carcinoma cells (PANC-1 cell line, (ATCC, catalogue #CRL-1469 were obtained from the American Tissue Culture Collection [ATCC, LGC Standards, UK])). PANC-1 cells were cultured in Dulbecco's Modified Eagle Medium (DMEM) supplemented with 10% fetal bovine serum (FBS) at 37°C and 5% CO_2. Cells were detached from cell T75 culture flasks with TrypLE TM (Gibco, Invitrogen, Oregon, USA) and diluted in supplemented media at a concentration of 6×10^4 cells/mL. Cells were then seeded in 24-well plate (Nunc, Fisher Scientific, Ireland) (3×10^4 cells/well) or 96-well plate (Nunc, Fisher Scientific, Ireland) (1.5×10^4 cells/well), depending on the experimental design. Cells were incubated for 24 hours to allow cell attachment to the plastic substrates prior to exposure to NPs. For the toxicity assessment the attention was focused on: (i) determination of the half-maximal lethal concentration (LC_{50}) at different concentrations of NPs (to find the concentration of NPs that can inhibit 50% of cell after a certain time of exposure); (ii) High Content Screening and Analysis (HCSA; Cytell GE Healthcare, USA) for analyzing different mechanisms involved in NPs-triggered cytotoxicity by monitoring early events in drug toxicity such as changes in mitochondrial membrane potential and lysosomal mass/pH, and Reactive Oxygen Species (ROS) formation; and (iii) Laser Scanning Confocal Microscopy (LSCM) which allows a qualitative analysis of cell uptake of nanoparticles for investigating if NPs were internalized into PANC-1 cells. All the tests

reported were performed in triplicate for 3 times, the results shown come from the average of the analysis carried out.

2.3.1 | LC_{50} evaluation

Nanoparticles were dispersed in supplemented DMEM medium by serial dilutions at concentrations ranging from 0 to the concentration for stock solution (equal to 5 mg/mL for Fe_3O_4 NPs and 5.6 mg/mL for SiO_2-Fe_3O_4 NPs). PANC-1 cells were exposed to NPs for 48 hours (n replicates = 2; n tests = 3). Untreated cells (negative control) and cells exposed to 70% acetone for 30 minutes (positive control) were also included in the experimental design. After 48 hours, PANC-1 cells were detached from the wells using 200 μL/well TrypLE™ Select (Gibco, Biosciences, Ireland) and transferred to Eppendorf containing 600 μL media. Cell counting was then carried out on the cell suspensions by flow cytometer (BD Accuri C6 Becton Dickinson Biosciences, UK), while keeping constant the counting time among samples. Cell population analysis was performed as for manufacturer's protocol. Briefly, the cells were visualized using the FSC-A vs FSC-H scatter plot and a gate was applied (P1) to exclude debris at lower scatter intensities and cell aggregates via doublet discrimination. A minimum of 10 000 events was collected in the (P1) gate for the negative control. Measurements for each sample were carried out on duplicates and are presented as average ± SD. Cell viability curves were fitted to such data by means of Prism, Graph-Pad software, USA, and reported in Figure 5. Half-maximal lethal concentration (LC_{50}), reported as average ± 95% confidence interval, were extrapolated from the curves thus obtained and used in subsequent HCSA experiments.

2.3.2 | High content screening and analysis (HCSA)

High content screening analysis is a reliable fluorescence microscopy technique for simultaneously analyzing different mechanisms involved in cytotoxicity (such as changes in mitochondrial membrane potential and lysosomal mass/pH, and Reactive Oxygen Species [ROS] formation) based on morphological and biochemical cellular features. The imaging where performed by the Cytell Cell Imaging System which scans and acquires the images directly from the well plate. Ten fields per well were acquired and quantified under brightfield and fluorescence intensity to account for cellular morphology and subcellular changes, respectively. Then the average intensity was calculated by processing the images with MATLAB software.

Changes in mitochondrial membrane potential and lysosomal mass/pH are critical cellular events correlated to cytotoxicity. Mitochondrial transmembrane potential changes were measured using a mitochondrial membrane potential dye, which accumulates in healthy mitochondria with intact membrane potential, and is absent from depolarized mitochondria that result from a cytotoxic compound such as valinomycin. Changes in lysosomal mass/pH were detected by mean of a fluorescent dye, which is a weak base and accumulates in lysosomes during cytotoxicity. Using Cytell Cell Images Analyzer is possible to notice changes in mitochondrial membrane or lysosomal mass/pH, which are recognizable thanks to the increase or decrease in the fluorescence intensity by changing the NPs concentrations. In fact, a change in lysosomal mass/pH, should show a fluorescence intensity increase for all NPs concentrations that are not toxic and a decrease for the toxic ones, which means that lysosome damage/dysfunction occurs. To identify a change in mitochondria membrane, instead, we should observe an intensity increase when metabolic activity increase and an intensity decrease when membrane damage occurs. PANC-1 cells were seeded at a density of 7.5×10^4 cells/mL (1.5×10^4 cells/well) in 96-well plate (Nunc, Fisher Scientific, Ireland) and incubated for 24 hours at 37°C, 5% CO_2. NPs were diluted in supplemented DMEM medium at concentrations equal to 0, 5, 50, 100, 200, and 400 μg/mL. PANC-1 cells were exposed to nanoparticles for 48 hours in duplicate (n replicates = 2; n tests = 3). Cells were also exposed to 120 μmol/L Valinomycin (200 μL) for 24 hours as the positive control for mitochondrial potential, and to 100 μmol/L Tacrine (200 μL) for 24 hours as the positive control for changes in lysosomal mass/pH. After 24 hours exposure, the appropriate Live Cell Staining Solution was added to each well for assaying changes in mitochondrial transmembrane potential, the Mitochondrial Membrane Potential Dye was used; for assaying changes in lysosomal mass or pH, the Lysosomal Mass/pH Dye was added to the staining solution. After 30 minutes of incubation, staining solutions were removed from the wells and 100 μL of Fixation Solution (3.7% formaldehyde) was added. Following 20 minutes incubation, cells were washed using 1× Wash Buffer and 100 μL Nuclear Staining Solution (5.5 μL Hoechst Dye diluted in 11 mL 1× Wash Buffer) was added and left for 30 minutes at 37°C covered with thin foil. After that, wells were washed twice with wash buffer and the plate was stored in the dark at 4°C before and after imaging.

Reactive Oxygen Species (ROS) formation can be directly monitored in real time using fluorescence microscopy, flow cytometry or HCSA. An elevated level of ROS is an important indicator of cellular stress and an accurate recording of this parameter would be very informative. As for lysosomal and mitochondria dysfunction, PANC-1 cells were seeded at a density of 7.5×10^4 cells/mL (1.5×10^4 cells/well) in a 96-well plate (Nunc, Fisher Scientific, Ireland) and incubated for 24 hours at 37°C, 5% CO_2. NPs

were diluted in supplemented DMEM medium at concentrations equal to 0, 5, 50, 100, 200, and 400 μg/mL. PANC-1 cells were exposed to nanoparticles for 48 hours in triplicate (n replicates = 3; n tests = 2). A positive control was also included in the experimental design: the oxidative activity was stimulated with H_2O_2 to a final concentration of 100 μmol/L for 24 hours. The staining solution was then prepared mixing 50 μL of 2′,7′-dichlorofluorescin diacetate (DCFDA) Dye with 40 μL of dimethylsulfoxide (DMSO) and then using 18.49 μL of Dye/DMSO mixed with 3.982 mL of PBS to a final concentration of 10 μmol/L. After 24 hours exposure, the Staining Solution was added to each well (200 μL/well). The cells were incubated for 45 minutes at 37°C, then the staining solution was removed and prewarmed growth medium was added. Plates were imaged by Cytell Cell Imaging System. This system scans all the images of the 96-well plate and then the fluorescence from the images is acquired to calculate the average intensity in each well (10 different field for each well were detected).

2.3.3 | Laser scanning confocal microscopy (LSCM)

Laser scanning confocal microscopy was used to determine the NPs uptake into the cell. PANC-1 cells were seeded at a density of 3×10^4 cells/well on chamber glass slides. Cells were incubated for 24 hours to allow attachment to the glass and then exposed to subcytotoxic concentrations of Fe_3O_4 NPs and SiO_2-Fe_3O_4 NPs (below the concentration estimated by LC_{50} calculations, 150 μg/mL), as determined by LC_{50} calculations. The NPs concentrations tested were equal to 40 μg/mL, in order to be sure that no toxic effect was triggered by cell exposure to the nanomaterials. After exposure for 24 hours, cells were fixed with 3.7% formaldehyde for 10 minutes at room temperature. PANC-1 cells were then incubated with 0.1% TritonX-100 (3 minutes, room temperature) followed by 1% bovine serum albumin (BSA) blocking buffer for 30 minutes. PANC-1 cells were then stained with rhodamine phalloidin (F-actin filament) and Hoechst (for nuclei) and left at room temperature for 1 hour in the dark. After that, wells were washed twice with PBS and the glass slide was mounted with a mounting medium and covered with a cover slip. Edges were sealed whit a clear nail polish. At the end the slide was stored in the dark at 4°C before and after the imaging.

2.3.4 | Statistical analysis

Statistical analysis was carried out with Tukey's method, in which the comparison between 2 samples was found using the Student T test. Each sample shown on the HCSA histograms, was compared with their respective negative control. $P < .05$ value was selected as significant ($^*P < .05$).

3 | RESULTS

3.1 | TEM, SAED, EDS

From a morphological point of view, both (bare Fe_3O_4 and SiO_2-Fe_3O_4) NPs demonstrate an almost spherical shape and dimensional range ranging approximately from 10 to 20 nm in size, as shown in Figure 1. Thickness of the SiO_2 shell was measured to be around 1 nm.

SAED patterns made on the obtained NPs (Figure 2) matched those reported for magnetite.[21] The pattern of SiO_2-Fe_3O_4 NPs is identical to the Fe_3O_4 NPs one because of the amorphous nature of the silica shell.[24]

The EDS spectra are shown in Figure 3A, B, and the atomic percentages of the element are reported in the insets.

3.2 | Colloidal stability

The behavior of the Fe_3O_4 NPs suspensions, with or without CA capping, after different times of sedimentation, in the presence or in the absence of an external magnetic field, as shown in Figure 4. In the absence of an external magnetic field, both naked Fe_3O_4 and CA capped Fe_3O_4 are stable at $t = 0$. After 48 hours a partial precipitation of Fe_3O_4 NPs is visible, while the CA capped NPs are still stable. A certain instability can be observed at $t = 0$ for the naked Fe_3O_4 NPs if an external magnet is applied at the bottom of the suspension. The precipitation of the Fe_3O_4

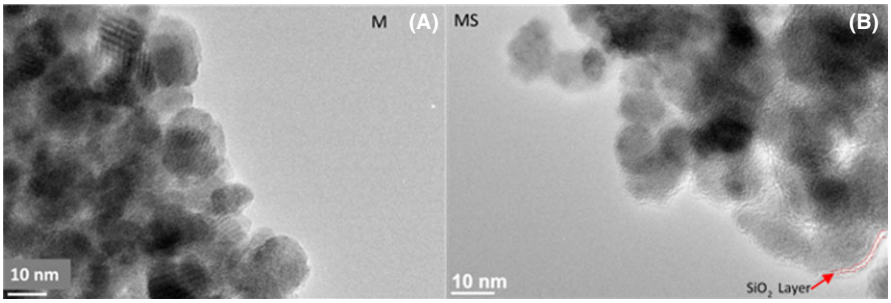

FIGURE 1 TEM images of Fe_3O_4 NPs (A) and SiO_2-Fe_3O_4 NPs (B) [Color figure can be viewed at wileyonlinelibrary.com]

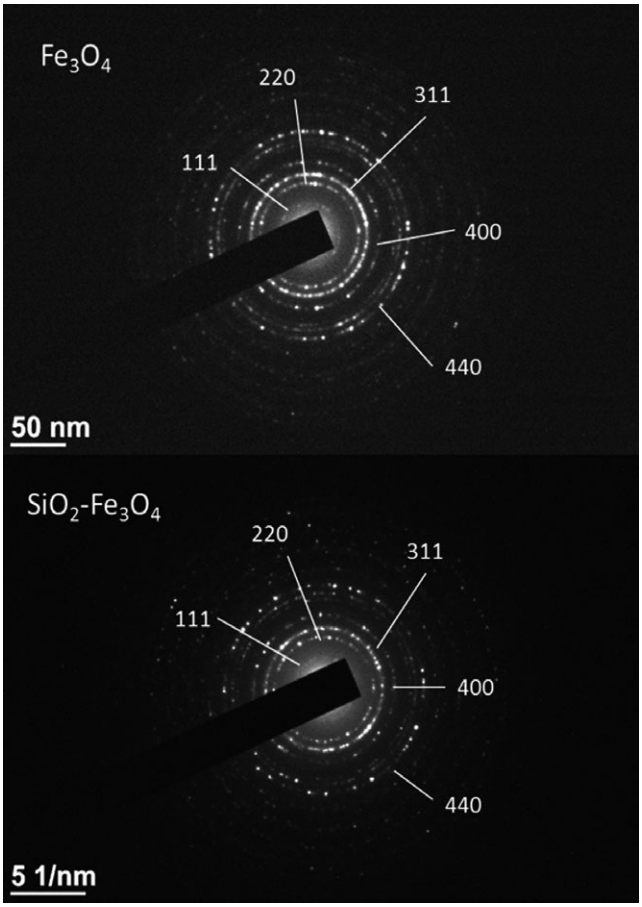

FIGURE 2 SAED patterns of Fe_3O_4 and SiO_2-Fe_3O_4 NPs

NPs is almost complete, in these conditions, after 48 hours. On the contrary, the CA capped Fe_3O_4 NPs present colloidal stability even under the action of the magnetic field both at $t = 0$ and $t = 48$ hours. Thus, the presence of the CA layer determined a very good dispersion of the NPs, allowing a controlled silica shell development during the subsequent Stöber synthesis.

The isoelectric point (IEP) of Fe_3O_4 NPs and SiO_2-Fe_3O_4 NPs are reported in Table 1. Both the NPs present an IEP in acidic range (at about 2 for Fe_3O_4 and 1.5 for SiO_2-Fe_3O_4). These values are in agreement with literature, taking into account that Fe_3O_4 NPs are capped with CA and that silica shell usually maintains the IEP value of Fe_3O_4 at acidic ranges.[25.]

3.3 | Colloid concentrations

Nanoparticle tracking analysis was used to determine the concentrations of the Fe_3O_4 and SiO_2-Fe_3O_4 NPs suspensions. The final concentrations (resulting from an average between all the data found out from the NTA repeated in triplicate) are of 5 and 5.6 mg/mL for Fe_3O_4 and for SiO_2-Fe_3O_4, respectively.

3.4 | Dynamic light scattering

The DLS results shown 2 important parameters defining the physico-chemical behavior of NPs in solutions: the Z-average size (hydrodynamic radius) and the PDI. An average hydrodynamic radius for Fe_3O_4 NPs of 17.56 ± 0.162 nm and for SiO_2-Fe_3O_4NPs of 10.92 ± 0.65 nm have been detected, while the PDI was 0.21 ± 0.01 and 0.38 ± 0.01, respectively.

3.5 | Magnetic characterization

The magnetic properties of the 2 kinds of SPIONs were investigated using a Vibrating Samples Magnetometer (VSM -Lakeshore). Both Fe_3O_4 and SiO_2-Fe_3O_4 NPs exhibited a superparamagnetic behavior since the hysteresis cycles (reported in Ref[13]) revealed no evidence of remanent magnetization and coercivity. The saturation magnetization (Ms) of uncoated Fe_3O_4 was 58 emu/g, while silica coating reduced

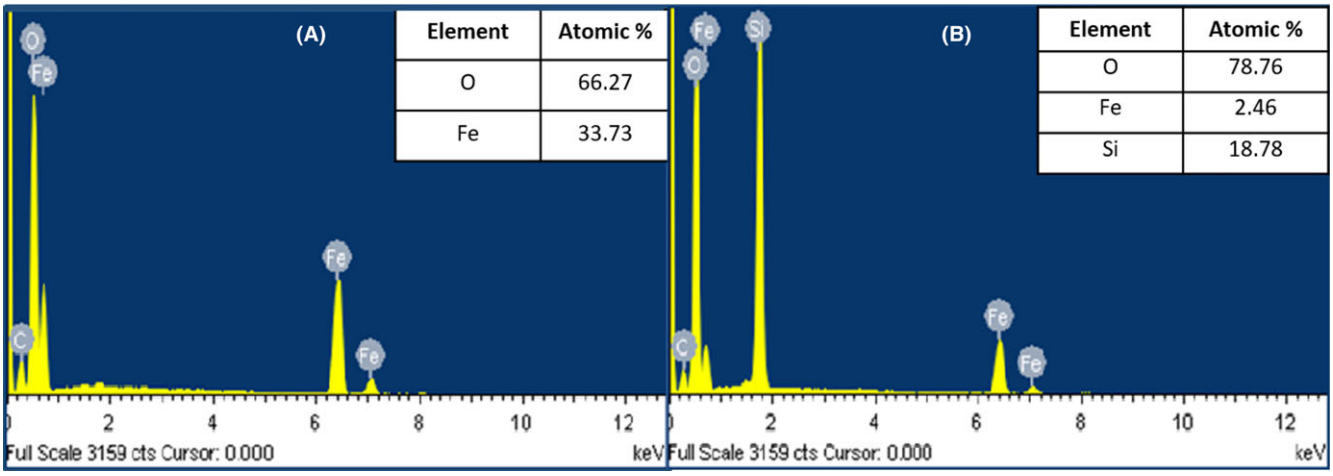

FIGURE 3 EDS on (A) Fe_3O_4 NPs and (B) SiO_2-Fe_3O_4 NPs samples with corresponding mean value composition. Spectrum taken from 1 μm^2 area [Color figure can be viewed at wileyonlinelibrary.com]

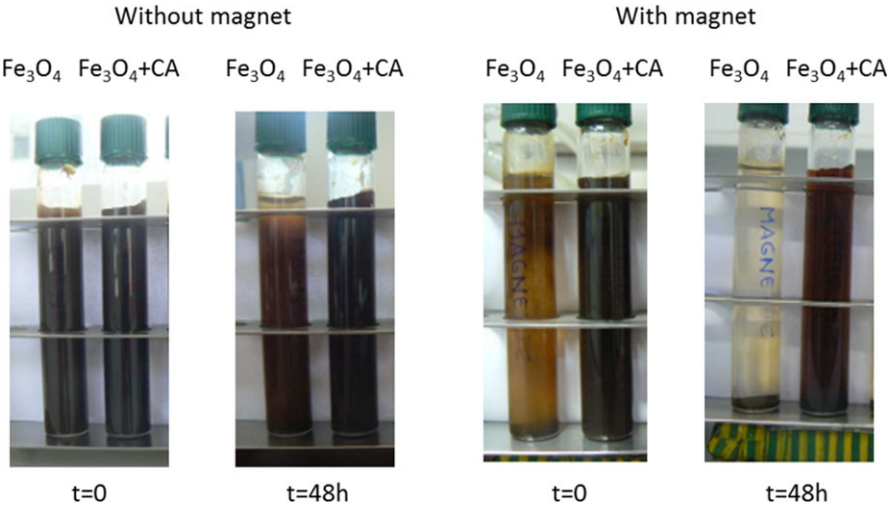

FIGURE 4 Sedimentation test on naked Fe_3O_4 and CA capped Fe_3O_4 NP [Color figure can be viewed at wileyonlinelibrary.com]

TABLE 1 The isoelectric point (IEP) and magnetization saturation (Ms) of CA capped Fe_3O_4 NPs and SiO_2-Fe_3O_4 NPs

Nanoparticles	Ms [emu/g]	IEP
Fe_3O_4	58	2
Fe_3O_4-SiO_2	31	1.5

Ms at 31 emu/g (Table 1). Considering that the 2 values are normalized to the NPs mass, we could hypothesize that the little decrease in Ms for the SiO_2-Fe_3O_4 NPs in comparison to uncoated Fe_3O_4 can be simply explained by the lower amount of Fe_3O_4 in the suspension. This is due to the weight of the sample that considers SiO_2 and Fe_3O_4 together. Qualitatively, no changes in the superparamagnetic properties of the core were detected after silica shell formation.

3.6 | In vitro tests

3.6.1 | Evaluation of lethal concentration (LC_{50})

The concentration of NPs that can cause the death of 50% of cell population, namely $LC_{50,}$ after 48 hours was found to be similar for both Fe_3O_4 and SiO_2-Fe_3O_4 NPs (about 150 μg/mL), as shown in Figure 5. This was found to be within a biologically accepted standard deviation for both materials, despite theSiO_2-Fe_3O_4 NPs shows a higher variance at the lower concentrations. This was found to be in line with previous work and the literature.

3.6.2 | High content screening and analysis (HCSA)

High Content Screening results for the Lysosomal and Mitochondria response are presented in Figures 6 and 7. In detail, the lysosomal dysfunction is shown by representative images and the graph reported in Figure 6.

Images (Figure 6A-D) show the fluorescence intensity of the cell exposed to Fe_3O_4 NPs concentrations of 5 μg/mL (C) and 400 μg/mL (D), compared to negative (A) and positive control (B) as example. The images reported are representative of the fluorescence signal detected in one random field.

The fluorescence intensity of cells exposed to SiO_2-Fe_2O_3 NPs is not shown for shortness because they are

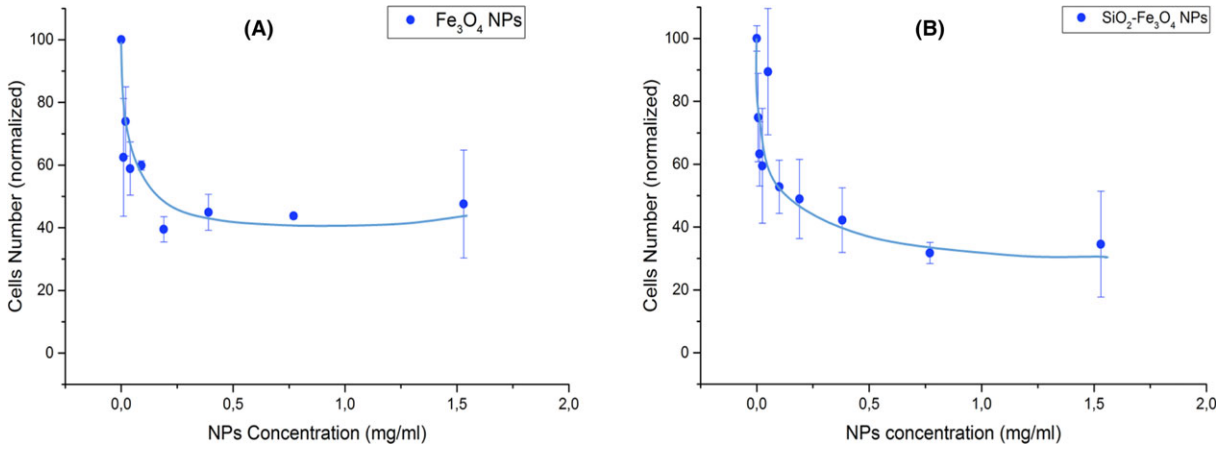

FIGURE 5 Evaluation of LC_{50} for Fe_3O_4 NPs (A) and SiO_2-Fe_3O_4 NPs (B) [Color figure can be viewed at wileyonlinelibrary.com]

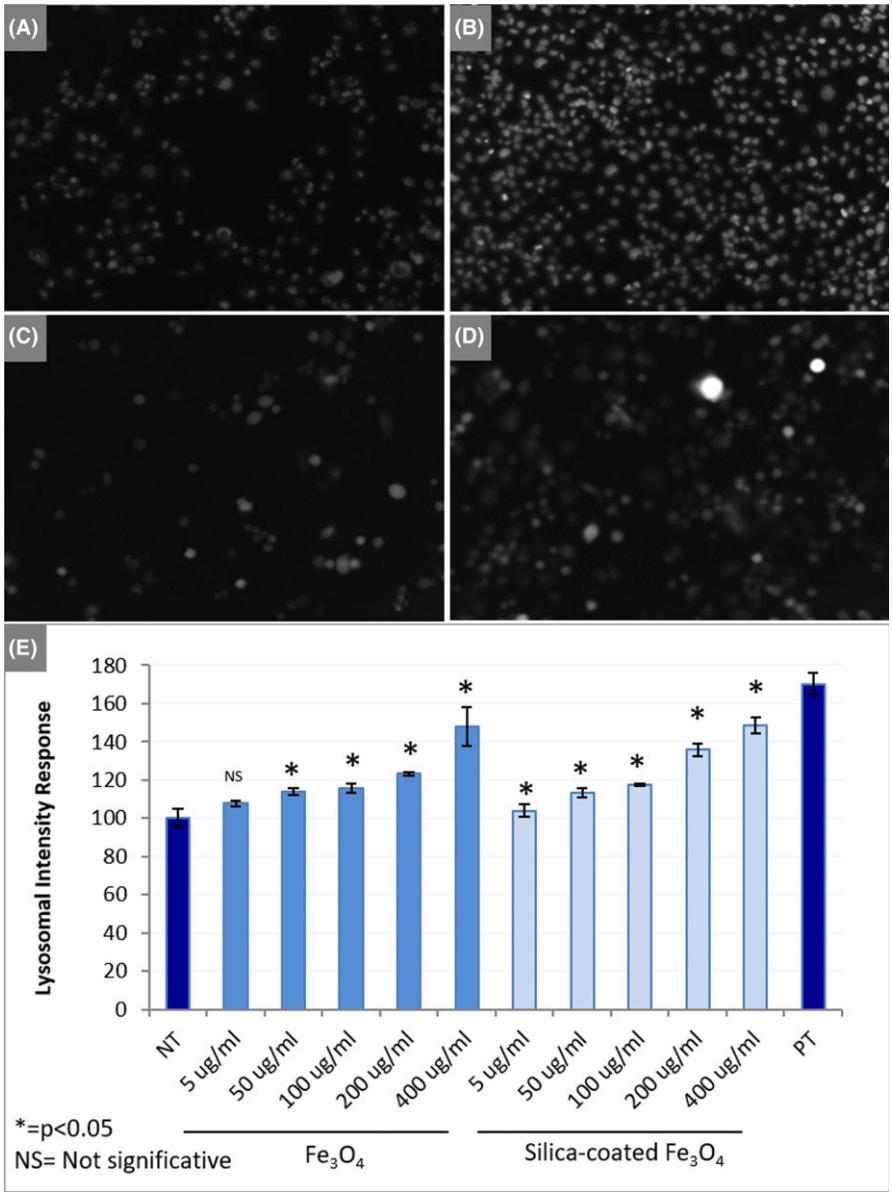

FIGURE 6 A, negative control (NT) for lysosomal activity (cells treated with media only); B, positive control (PT) (cells treated with 100 μmol/L Tacrine for 24 h); C, Lysosomal response with Fe_3O_4 NPs exposure at 5 μg/mL; D, Lysosomal response with Fe_3O_4 NPs exposure at 400 μg/mL; E, Changes in Lysosomal mass/pH in relations with different Fe_3O_4 and SiO_2-Fe_3O_4 NPs concentrations; Optical Magnification = 10×. Statistical analysis were carried out through Student *t* test between NT and all the NPs concentration; *Significant for $P < .05$; NS, Not statistically Significant [Color figure can be viewed at wileyonlinelibrary.com]

similar to those already represented. The graph (E) reports the changes in lysosomal mass/pH following exposure of PANC-1 cells, in relations with the different NPs concentrations (both Fe_2O_3 and SiO_2-Fe_2O_3). The histogram presented is based on the average of all the processed images ($n_{tests} = 3$ $n_{replicates} = 3$). A decrease in the pH or increase in lysosome number or mass, caused by compound toxicity, produced a fluorescence intensity rise. Increase in pH or decrease in lysosome number or mass, caused a decrease in staining intensity. Negative and positive controls are also included in the graph.

Representative images showing different intensity for mitochondria dysfunction when the cells are exposed to Fe_3O_4 NPs concentrations of 5 and 400 μg/mL (C-D), compared to negative and positive control (A-B) as example, are shown in Figure 7A-D. The intensity for mitochondria dysfunction in cells exposed to SiO_2-Fe_3O_4 NPs is not shown for shortness because they are similar to those already reported. The graph (Figure 7E) shows the mitochondria activity following exposure of PANC-1 cells, in relations with the different NPs concentrations (both Fe_2O_3 and SiO_2-Fe_2O_3). The graph (which is based on the average of all the acquired fields) shows no intensity increase when cells are exposed to increasing NPs concentrations, conversely to the above-reported lysosomal activity. Positive and negative controls are also included in the graph for comparison.

3.6.3 | HCSA for ROS detection

Reactive Oxygen Species reaction was assessed by High Content Screening by mean fluorescence DFDA staining. Four different images of the fluorescence captured from negative (Figure 8A) and positive control (Figure 8B) and

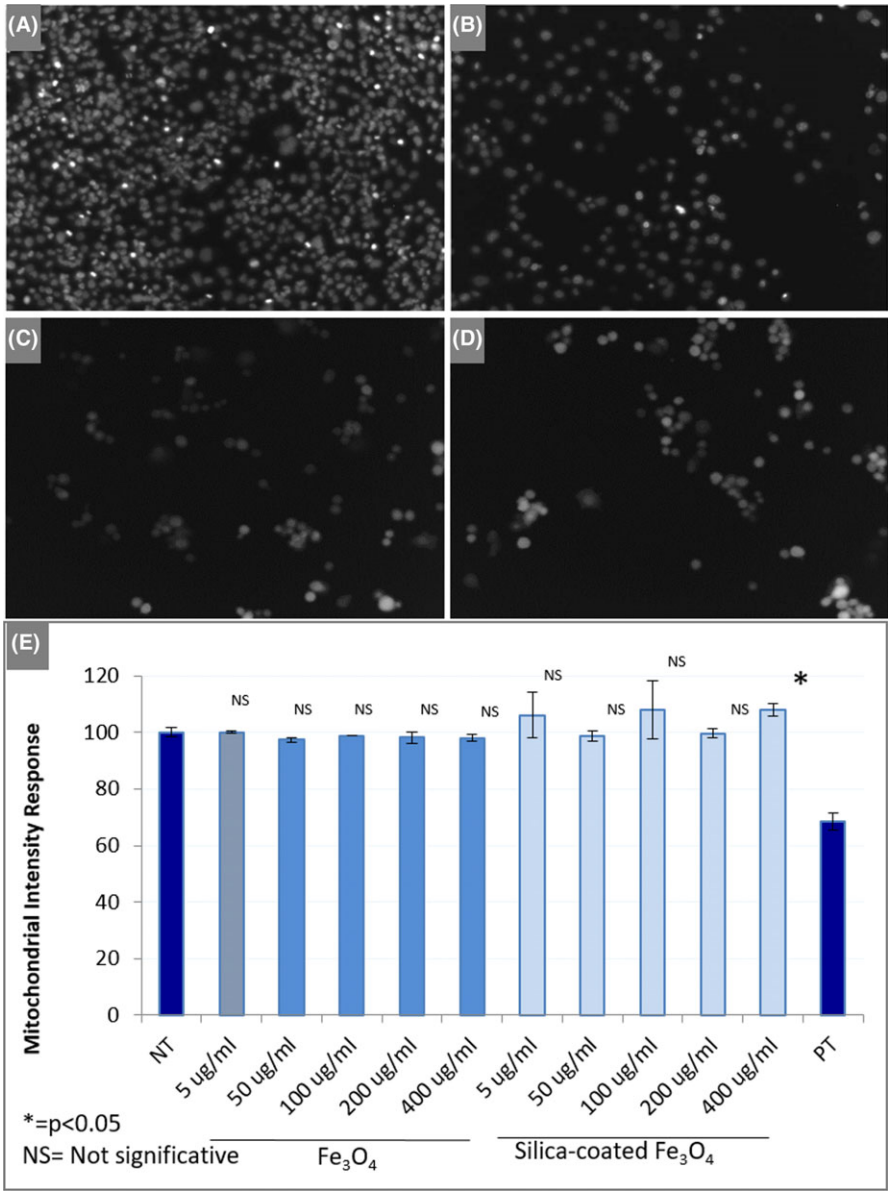

FIGURE 7 A, negative control (NT) for mitochondria dysfunction (cells treated with media only); B, image of the positive control (PT) (cells treated with 120 μmol/L valinomycine for 24 hours); C, Mitochondrial response with Fe_3O_4 NPs exposure at 5 μg/mL; D, Mitochondrial response with Fe_3O_4 NPs exposure at 400 μg/mL; E, Mitochondria Dysfunction in relations with different Fe_3O_4 and SiO_2-Fe_3O_4 NPs concentrations; The magnification used for these images was 10×. Statistical analysis were carried out through Student *t* test between NT and all the NPs concentration; *Significant for $P < .05$; NS, Not statistically Significant [Color figure can be viewed at wileyonlinelibrary.com]

an example of the emission of Fe_3O_4 NPs at 5 and 400 μg/mL (Figure 8C, D, respectively). The fluorescence of SiO_2-Fe_3O_4 NPs is not reported for brevity. The graph (Figure 8E) shows the response from the ROS detection following the exposure of PANC-1 cells, in relations with the different Fe_3O_4 and SiO_2-Fe_3O_4 NPs concentrations (all the histogram columns come from the average of the processed images). An increase in intensity shows that an elevated level of ROS exists, and this indicates cellular stress, while a decrease means that no cellular stress is occurred. Negative (NT) and Positive (PT) control are also included in the graph.

3.6.4 | Laser scanning confocal microscopy

Confocal microscopy was used to investigate the internalization of both NPs, as shown in Figure 9. The planar and z-stack microscopy analysis of both Fe_3O_4 NPs and SiO_2-Fe_3O_4 NPs provided the evidence of cellular uptake. Using the high-refractive index of the 2 metallic particles, it was possible to detect them without using any fluorescent dye, which is known to modify the particle behavior. From the analysis of the stacks of images it was possible to track the presence of NP, or cluster of them, internalized into the PANC-1 cells, as shown in each orthogonal section taken on the 3 images.

4 | DISCUSSION

The main aim of this study was to compare the cytotoxic response against PANC-1 cells of 2 different SPIONs, pure magnetite NPs (Fe_3O_4) and silica-coated magnetite (SiO_2-Fe_3O_4) NPs, with particular emphasis on estimating the

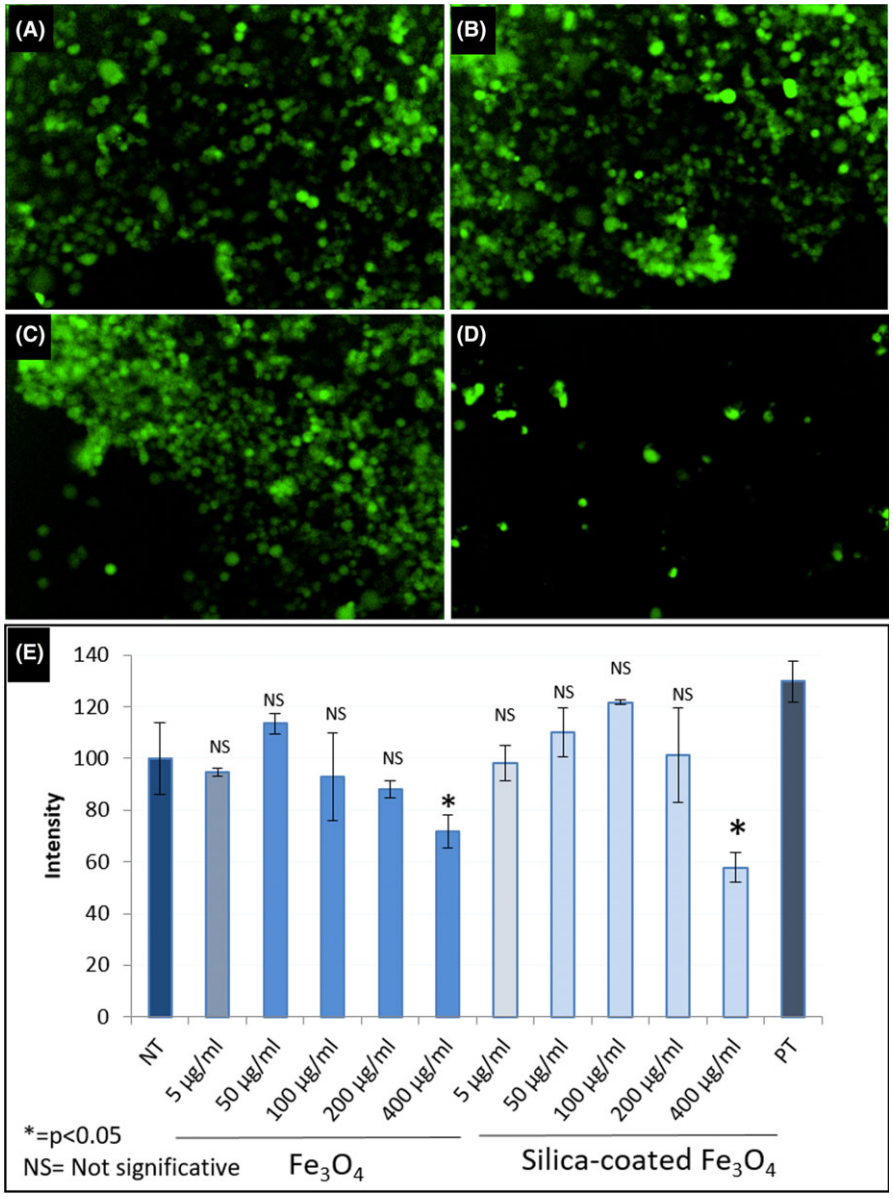

FIGURE 8 Representative images reporting the Reactive Oxygen Species quantification (A-D). Fluorescence images reports the negative (NT) (A) and positive (PT) (B) control and of Fe_3O_4 NPs at the concentration of 5 μg/mL (C) and 400 μg/mL (D); E, graph showing the change in intensity related to the Fe_3O_4 and SiO_2-Fe_3O_4 NPs concentrations. Magnification used: 10×. Statistical analysis were carried out through Student *t* test between NT and all the NPs concentration; *Significant for $P < .05$; NS, Not statistically Significant [Color figure can be viewed at wileyonlinelibrary.com]

role of the silica coating in the biological responses detected. This investigation was performed using different techniques to understand if any toxicity is measurable and at which dose. First, Fe_3O_4 and SiO_2-Fe_3O_4 NPs were synthetized by a protocol optimized by the authors[10] and characterized from the physical and chemical point of view, to understand their size, shape, morphologies, and compositions. The average dimension of all NPs was determined by TEM observations and the hydrodynamic size recorded by DLS. From morphological analysis an average size of 10-20 nm has been detected for all the NPs. The hydrodynamic size calculated by DLS was 17.56 nm for Fe_3O_4 NPs and 10.92 nm for the SiO_2-Fe_3O_4 NPs. The slightly lower size detected by DLS for the SiO_2-Fe_3O_4 NPs is probably due to a certain residual aggregation tendency of the uncoated Fe_3O_4 NPs,[26] which can be overcome by the silica-coating process. This hypothesis is supported by the higher PDI detected for SiO_2-Fe_3O_4 NPs, as an index of a higher polydispersion. As reported by several works,[27] nanoparticles in this size range could diffuse through the blood vessel endothelium, penetrate through the tissues and avoid removal by Mononuclear Phagocytic System (MPS).

The superparamagnetic behavior of both, Fe_3O_4 and SiO_2-Fe_3O_4 NPs, were confirmed as the absence of any remanent magnetization and coercivity at room temperature.[13] Furthermore, colloidal stability of NPs after 48 hours was confirmed with the suspension stability test with and without the presence of the external magnetic field, as shown in Figure 4.

The cytotoxicity test of NPs on PANC-1 cells was performed by different methods.[28,29] First, the LC_{50} results show that after 48 hours of exposure the toxicity for both SiO_2-Fe_3O_4 NPs and Fe_3O_4 NPs (around 150 μg/mL) was within a biologically accepted standard

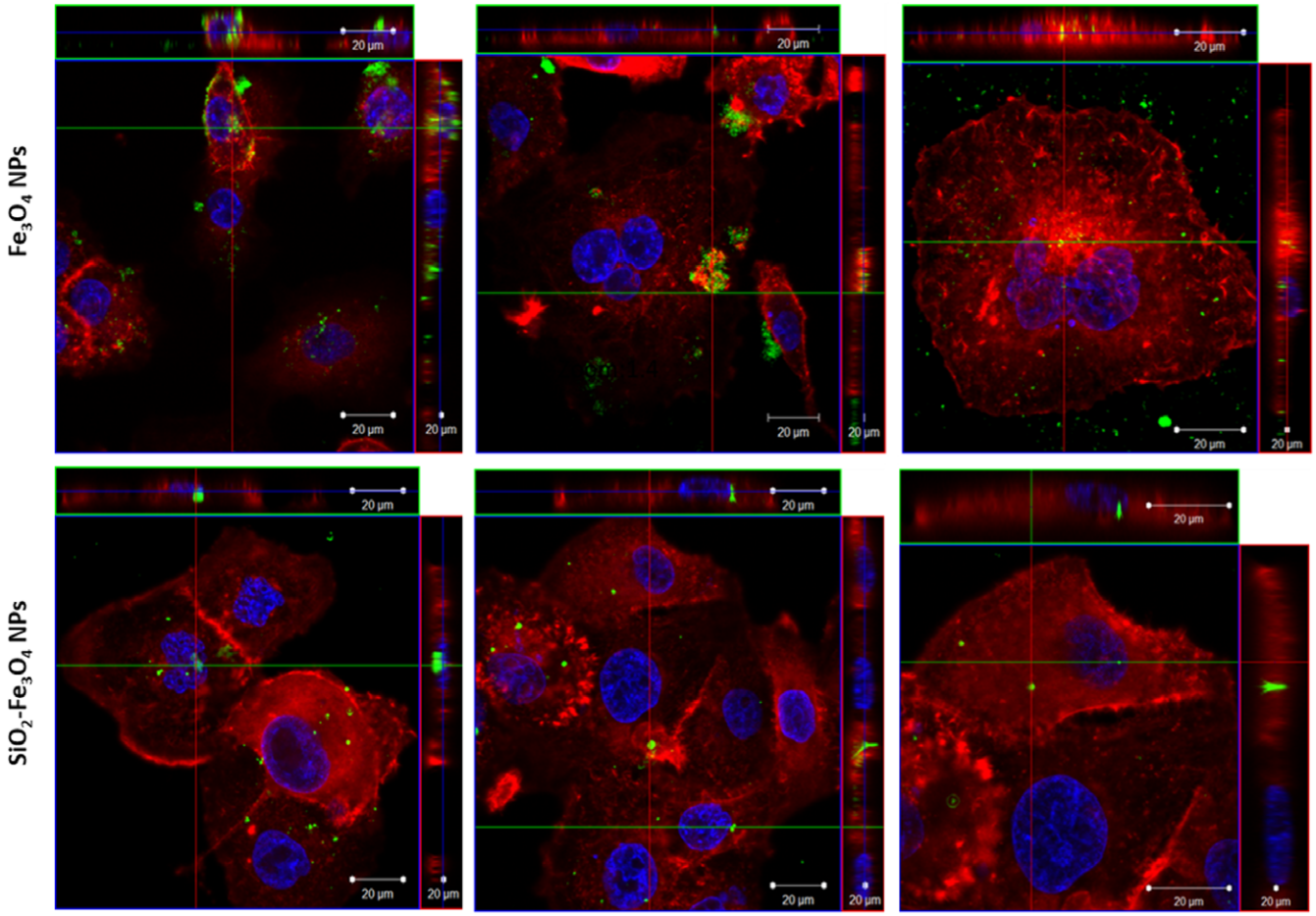

FIGURE 9 Representative images reporting cellular internalization of Fe_3O_4 on the top and SiO_2-Fe_3O_4 on the bottom. The images show 3 different fields of the same well with a magnification of 63×. Panc-1 cells were stained with rhodamine phalloidin (F-actin filaments, in red); Hoechst 33342® (nuclei, in blue); NPs (green fluorescence). Scale bar: 20 µm [Color figure can be viewed at wileyonlinelibrary.com]

deviation for both materials (see Figure 5), despite the SiO_2-Fe_3O_4 NPs show a higher variance in the low concentrations, which is comparable with previous literature.[30] According to the literature, the SiO_2 coating, by Stöber methods, is providing a biocompatible layer that allows the exploitation of the particles for multiple biomedical applications.[30,31]

High content screening analysis experiments allowed analyzing some of the numerous subcellular mechanisms involved in NPs-triggered cytotoxicity. HCSA enabled the early registration of toxicity, almost at the limit of Non-observable adverse effect (NOAL). These have been monitored as changes in mitochondrial membrane potential, lysosomal mass/pH, and Reactive Oxygen Species (ROS) formation. From these results, it is possible to understand how the toxicity changes by increasing concentrations. In particular, the change of intensity detected during the test for the different concentrations is shown. Concerning the lysosomal mass/pH response as shown in (Figure 6) the intensity may decrease for all the NPs concentrations that are not toxic, whereas any increase would represent a lysosome damage or dysfunctional response. The positive control (Tacrine), shown in Figure 6A, is higher than the negative control (Figure 6B). This is expected because tacrine induces changes in lysosomal mass, which is an early indicator of cell toxicity. Cells exposed to tacrine (100 µmol/L) demonstrated an increase in the number of lysosomes, so an increase in the intensity, indicating toxicity. The graph on Figure 6E shows an increase in intensity by raising the concentration for both Fe_3O_4 and SiO_2-Fe_3O_4; this could be due to an increase in the number of lysosome or a decrease in lysosomal pH, that raise consequentially the intensity. Concerning the Mitochondria response, a signal increase would be representative of an increasing metabolic activity, whereas a decrease would be indicative of a membrane damage. In Figure 7E the values of Mitochondria response are not showing significant changes regardless the concentration; on the contrary valinomycin decreases the intensity of staining since valinomycin negatively affects the integrity of the cell membrane. A possible hypothesis is that the NPs concentrations tested are not subjecting the cell to mitochondria stress, in fact

the fluorescence result to be almost unchanged for all doses of NPs, for both Fe_3O_4 and SiO_2-Fe_3O_4, with a slight variation in the latter.

In the literature, the cytocompatibility of Fe_3O_4 and Fe_3O_4-SiO_2 NPs, was tested on several different cell lines and using different assays. In particular, the NPs toxicity in a concentration-dependent mode was reported by also many authors.[10,13,32,33] Moreover, no significant difference in cytotoxic effect between Fe_3O_4 and Fe_3O_4-SiO_2 was also evidenced by some of the authors of this work. As example, Muzio et al,[11] using mouse breast cancer 4T1 cells and pancreatic islet endothelial MS1 cells, evidenced that the viability of 4T1 cells was not reduced in the presence of both Fe_3O_4 and Fe_3O_4-SiO_2 NPs and both NPs highly interact with MS1 cells, but no decrease in viability was induced. Borroni et al,[13] incubated MS1 cells, in static exposure conditions, with increasing doses of Fe_3O_4 and Fe_3O_4-SiO_2 NPs (from 2.5 to 80 μg/mL) for 48 hours and analyzed by MTT assay. In these conditions a slight or no reduction in cell viability was observed at 20 μg of NPs/mL for both Fe_3O_4 and Fe_3O_4-SiO_2 NPs. The NPs internalization was evaluated after 24 hours incubation with cells by Prussian blue iron staining, showing that NPs were present inside the cells, around the nuclei.

The ROS data presented as real time reactive oxygen production in PANC-1 is shown in Figure 8E; there, it is possible to observe a change in intensity in dependence of the nanoparticles concentrations. At low levels of ROS production, cells initiate a protective response to guarantee their survival; whereas an excess of ROS can damage cellular compounds such as membranes and various organelles, or directly cause genotoxicity. Thus, an elevated level of ROS is an important indicator of cellular stress. The graph shows, for Fe_3O_4 NPs and SiO_2-Fe_3O_4 NPs, in inverse proportion between the concentration of the nanoparticles vs the fluorescence associated with the ROS production. In particular, for the Fe_3O_4 NPs at around 50-100 μg/mL, the decrease in fluorescence marked the onset of cell death, confirmed by the lysosomal data. Whereas for the SiO_2-Fe_3O_4 NPs the onset for such cell death occurs at double the concentration of Fe_3O_4 NPs. An explanation for this response is linked to the fact, the passivated metal oxide layer of the Fe_3O_4 NPs is directly interacting with the PANC-1 cells to therefore promote the production ROS and therefore apoptotic death. Whereas a delay in ROS production is seen when the PANC-1 cells are exposed to SiO_2-Fe_3O_4 NPs when the passivation of the silica is then interacting with the cells.

Confocal microscopy was used to investigate the NPs internalization, as shown in Figure 9, where cellular uptake was addressed since it is most commonly used for drug delivery (for instance certain antimicrobial and antitumor drugs[34] have to pass through the cell membrane before acting their functions on the subcellular sites). From this analysis, it was evidenced that both Fe_3O_4 NPs and SiO_2-Fe_3O_4 NPs were able to pass through the membrane and accumulate intracellularly. This ability was particularly evident for SiO_2-Fe_3O_4 NPs, which, according to DLS measurements and sedimentation test, resulted better dispersed than the Fe_3O_4 NPs.

5 | CONCLUSIONS

The aim of the present work was to investigate the response of 2 different SPIONS (Fe_3O_4 and SiO_2-Fe_3O_4 NPs) when exposed in a concentration dose range in pancreatic cancer cells. Summarizing, the prepared NPs show dimension, shape, and morphology suitable for biomedical applications.

All the data presented in this work can be summarized as follows:

1. SPIONs have been produced by co-precipitation and Stöber methods.
2. SPIONs had an average size between 10 and 20 nm, in particular the SiO_2-Fe_3O_4 NPs results to be better dispersed than Fe_3O_4 NPs (showing a hydrodynamic diameter of 10.92 ± 0.65 nm vs 17.56 ± 0.16 nm)
3. Both NPs results to be superparamagnetic and colloidally stable, this feature making them suitable for biomedical contest.
4. SiO_2 coating represents a versatile material for surface functionalization to enable many biomedical applications.
5. The Confocal Microscopy showed particle uptake inside cell membrane, predominantly for SiO_2-Fe_3O_4 NPs.
6. The LC_{50} determination shows that comparable concentrations of SiO_2-Fe_3O_4 and Fe_3O_4 (150 μg/mL) are necessary to have detrimental effect on PANC-1 cells.
7. The HCSA test revealed similar cytotoxicity for Fe_3O_4 and SiO_2-Fe_3O_4 NPs.
8. Internalization was effective for both Fe_3O_4 and SiO_2-Fe_3O_4 NPs.

Taken into account these results, we can assume that this family of NPs could represent a promising tool for imaging and drug delivery and therefore as potential theranostics carrier for tackling the clinical unmet needs posed by pancreatic cancer as highlighted in many studies[35] and funded projects such as EC-FP7-MULTIFUN and EC-H2020-NOCANTHER to mention the most promising projects focused in translating and scaling up SPIONS for the treatment of pancreatic cancer.

ACKNOWLEDGMENTS

This research has been partially funded by the MULTIFUN project "Development of nanotechnology-based systems for detection, diagnosis and therapy for cancer" (ref #262943), the AIRC Grant 2012 "Development of engineered magnetic nanoparticles for cancer therapy" (PI AF, IG n. 13166) and by the S. Paolo Grant "CSP-Torino-Piemonte" 2012 "Development of engineered magnetic nanoparticles for targeted therapies (LV-MNPs)" (PI AF, 12-CSP-C04-018).

ORCID

Cristina Multari http://orcid.org/0000-0002-6395-8692
Marta Miola http://orcid.org/0000-0002-1440-6146
Sara Ferraris http://orcid.org/0000-0001-8316-5406
Dania Movia http://orcid.org/0000-0001-6412-8132

Kristina Žužek Rožman http://orcid.org/0000-0003-2652-1966
Antonia Follenzi http://orcid.org/0000-0001-9780-300X

Enrica Verné http://orcid.org/0000-0002-8649-4739
Adriele Prina-Mello http://orcid.org/0000-0002-4371-2214

REFERENCES

1. Vatta LL, Sanderson RD, Koch KR. Magnetic nanoparticles: properties and potential applications. *Adv Mater*. 2006;78:1793-1801.
2. Ficko BW, Nadar PM, Hoopes PJ, Diamond SG. Development of a magnetic nanoparticle susceptibility magnitude imaging array. *Phys Med Biol*. 2014;59:1047-1071.
3. Mbeh DA, Mireles LK, Stanicki D, et al. Human alveolar epithelial cell responses to core-shell superparamagnetic iron oxide nanoparticles (SPIONs). *Langmuir*. 2015;31:3829-3839.
4. Kolhatkar AG, Jamison AC, Litvinov D, Willson RC, Lee TR. Tuning the magnetic properties of nanoparticles. *Int J Mol Sci*. 2013;14:15977-16009.
5. Xu J-KK, Zhang F-FF, Sun J-JJ, Sheng J, Wang F, Sun M. Bio and nanomaterials based on Fe_3O_4. *Molecules*. 2014;19:21506-21528.
6. Gao J, Gu H, Xu B. Multifunctional magnetic nanoparticles: design, synthesis, and biomedical applications. *Acc Chem Res*. 2009;42:1097-1107.
7. Zeinali Sehrig F, Majidi S, Nikzamir N, Nikzamir N, Nikzamir M, Akbarzadeh A. Magnetic nanoparticles as potential candidates for biomedical and biological applications. *Artif Cells Nanomed Biotechnol*. 2016;44:918-927.
8. Dissanayake NM, Current KM, Obare SO. Mutagenic effects of Iron oxide nanoparticles on biological cells. *Int J Mol Sci*. 2015;16:23482-23516.
9. Nadeem K, Ali L, Gul I, Rizwan S, Mumtaz M. Effect of silica coating on the structural, dielectric, and magnetic properties of maghemite nanoparticles. *J Non Cryst Solids*. 2014;404:72-77.
10. Catalano E, Miola M, Ferraris S, et al. Magnetite and silica-coated magnetite nanoparticles are highly biocompatible on endothelial cells in vitro. *Biomed Phys Eng express*. 2016;3:025015.
11. Muzio G, Miola M, Ferraris S, et al. Innovative superparamagnetic iron-oxide nanoparticles coated with silica and conjugated with linoleic acid: effect on tumor cell growth and viability. *Mater Sci Eng, C*. 2017;76:439-447.
12. Prina-Mello A, Crosbie-Staunton K, Salas G, PuertoMorales M, Volkov Y. Multiparametric toxicity evaluation of SPIONs by high content screening technique: identification of biocompatible multifunctional nanoparticles for nanomedicine. *IEEE Trans Magn*. 2014;49:377-382.
13. Borroni E, Miola M, Ferraris S, et al. Tumor targeting by lentiviral vectors combined with magnetic nanoparticles in mice. *Acta Biomater*. 2017;59:303-316.
14. Jaidev LR, Chellappan DR, Bhavsar DV, et al. Multi-functional nanoparticles as theranostic agents for the treatment & imaging of pancreatic cancer. *Acta Biomater*. 2017;49:422-433.
15. Zhu L, Staley C, Kooby D, El-Rays B, Mao H, Yang L. Current status of biomarker and targeted nanoparticle development: the precision oncology approach for pancreatic cancer therapy. *Cancer Lett*. 2017;388:139-148.
16. Trabulo S, Aires A, Aicher A, Heeschen C, Cortajarena AL. Multifunctionalized iron oxide nanoparticles for selective targeting of pancreatic cancer cells. *Biochim Biophys Acta*. 2017;1861:1597-1605.
17. McCarroll J, Teo J, Boyer C, Goldstein D, Kavallaris M, Phillips PA. Potential applications of nanotechnology for the diagnosis and treatment of pancreatic cancer. *Front Physiol*. 2014;5:2.
18. Yallapu MM, Ebeling MC, Khan S, et al. Novel curcumin-loaded magnetic nanoparticles for pancreatic cancer treatment. *Mol Cancer Ther*. 2013;12:1471-1480.
19. Siegel RL, Miller KD, Jemal A. Cancer statistics, 2017. *CA Cancer J Clin*. 2017;67:7-30.
20. Campelj S, Makovec D, Drofenik M. Preparation and properties of water-based magnetic fluids. *J Phys Condens Matter*. 2008;20:204101.
21. Deng YH, Wang CC, Hu JH, Yang WL, Fu SK. Investigation of formation of silica-coated magnetite nanoparticles via sol-gel approach. *Colloids Surf A Physicochem Eng Asp*. 2005;262:87-93.
22. Maguire CM, Sillence K, Roesslein M, et al. Benchmark of nanoparticle tracking analysis on measuring nanoparticle sizing and concentration. *J Micro NanoManuf*. 2017;5:41002-41010.
23. Hole P, Sillence K, Hannell C, Manus C. Interlaboratory comparison of size measurements on nanoparticles using nanoparticle tracking analysis (NTA). *J Nanopart Res*. 2013;15:2101.
24. Hui C, Shen C, Tian J, et al. Core-shell Fe_3O_4 @ SiO_2 nanoparticles synthesized with well-dispersed hydrophilic Fe_3O_4 seeds. *Nanoscale*. 2011;3:701-705.
25. Sun Z, Su F, Forsling W, Samskog P-O. Surface characteristics of magnetite in aqueous suspension. *J Colloid Interface Sci*. 1998;197:151-159.
26. Lim J, Yeap S, Che H, Low S. Characterization of magnetic nanoparticle by dynamic light scattering. *Nanoscale Res Lett*. 2013;8:381.
27. Gaumet M, Vargas A, Gurny R, Delie F. Nanoparticles for drug delivery: the need for precision in reporting particle size parameters. *Eur J Pharm Biopharm*. 2008;69:1-9.

28. Singh A, Dilnawaz F, Mewar S, Sharma U, Jagannathan NR, Sahoo SK. Composite polymeric magnetic nanoparticles for co-delivery of hydrophobic and hydrophilic anticancer drugs and MRI imaging for cancer therapy. *ACS Appl Mater Interfaces*. 2011;3:842-856.
29. Wang X, Xing X, Zhang B, Liu F, Cheng Y, Shi D. Surface engineered antifouling optomagnetic SPIONs for bimodal targeted imaging of pancreatic cancer cells. *Int J Nanomedicine*. 2014;9:1601-1615.
30. Malvindi MA, De-Matteis V, Galeone A, et al. Toxicity assessment of silica coated iron oxide nanoparticles and biocompatibility improvement by surface engineering. *PLoS ONE* 2014;9:e85835.
31. Alwi R, Telenkov S, Mandelis A, et al. Silica-coated super paramagnetic iron oxide nanoparticles (SPION) as biocompatible contrast agent in biomedical photoacoustics. *Biomed Opt Express*. 2012;3:2500-2509.
32. Patila RM, Thorat ND, Shete PB, et al. Comprehensive cytotoxicity studies of superparamagnetic iron oxide nanoparticles. *Biochem Biophys Rep*. 2018;13:63-72.
33. Naqvi S, Samim M, Abdin M, et al. Concentration-dependent toxicity of iron oxide nanoparticles mediated by increased oxidative stress. *Int J Nanomedicine*. 2010;5:983-989.
34. Moscow J, Morrow CS, Cowan KH. General mechanisms of drug resistance. In: Kufe DW, Pollock RE, Weichselbaum RR, Bast RC, Gansler TS, Holland JF, Frei E, eds. *Holland-Frei Cancer Medicine*, 6th edn; Hamilton, ON: BC Decker; 2003:762. https://www.ncbi.nlm.nih.gov/books/NBK12424/#A11388.
35. Gobbo OL, Sjaastad K, Radomski MW, Volkov Y, Prina-Mello A. Magnetic nanoparticles in cancer theranostics. *Theranostics*. 2015;5:1249-1263.

How to cite this article: Multari C, Miola M, Ferraris S, et al. Synthesis and characterization of silica-coated superparamagnetic iron oxide nanoparticles and interaction with pancreatic cancer cells. *Int J Appl Ceram Technol*. 2018;15:947–960. https://doi.org/10.1111/ijac.12897